

The VIMOS-VLT Deep Survey[★]

Beyond color bimodality: the mix of galaxy populations up to $z \sim 2$

P. Franzetti¹, M. Scodeggio¹, D. Maccagni¹, B. Garilli¹, D. Vergani¹, L. Guzzo², L. Tresse³, O. Ilbert⁴, F. Lamareille⁵, T. Contini⁵, O. Le Fèvre³, G. Zamorani⁶, J. Brinchmann⁷, S. Charlot⁸, D. Bottini¹, V. Le Brun³, J.P. Picat⁵, R. Scaramella^{9,10}, G. Vettolani⁹, A. Zanichelli⁹, C. Adami³, M. Arnaboldi¹¹, S. Arnouts³, S. Bardelli⁶, M. Bolzonella⁶, A. Cappi⁶, P. Ciliegi⁶, S. Foucaud¹², I. Gavignaud^{5,13}, A. Iovino², H.J. McCracken^{8,14}, B. Marano¹⁵, C. Marinoni³, A. Mazure³, B. Meneux^{1,2}, R. Merighi⁶, S. Paltani^{16,17}, R. Pellò⁵, A. Pollo³, L. Pozzetti⁶, M. Radovich¹¹, E. Zucca⁶, O. Cucciati^{2,18}, and C.J. Walcher³

¹ 1 INAF - IASF Milano, via Bassini 15, I-20133, Milano, Italy
e-mail: paolo@lambrate.inaf.it

² 2 INAF - Osservatorio Astronomico di Brera, Via Brera 28, Milano, Italy

³ 3 Laboratoire d'Astrophysique de Marseille, UMR 6110 CNRS-Université de Provence, BP8, 13376 Marseille Cedex 12, France

⁴ 4 Institute for Astronomy, 2680 Woodlawn Dr., University of Hawaii, Honolulu, Hawaii, 96822

⁵ 5 Laboratoire d'Astrophysique de l'Observatoire Midi-Pyrénées (UMR 5572), 14, avenue E. Belin, F31400 Toulouse, France

⁶ 6 INAF - Osservatorio Astronomico di Bologna, Via Ranzani, 1, I-40127, Bologna, Italy

⁷ 7 Centro de Astrofísica da Universidade do Porto, Rua das Estrelas, 4150-762 Porto, Portugal

⁸ 8 Institut d'Astrophysique de Paris, UMR 7095, 98 bis Bvd Arago, 75014 Paris, France

⁹ 9 INAF - IRA, Via Gobetti, 101, I-40129, Bologna, Italy

¹⁰ 10 INAF - Osservatorio Astronomico di Roma, Via di Frascati 33, I-00040, Monte Porzio Catone, Italy

¹¹ 11 INAF - Osservatorio Astronomico di Capodimonte, Via Moiariello 16, I-80131, Napoli, Italy

¹² 12 School of Physics & Astronomy, University of Nottingham, University Park, Nottingham, NG72RD, UK

¹³ 13 European Southern Observatory, Karl-Schwarzschild-Strasse 2, D-85748 Garching bei München, Germany

¹⁴ 14 Observatoire de Paris, LERMA, 61 Avenue de l'Observatoire, 75014 Paris, France

¹⁵ 15 Università di Bologna, Dipartimento di Astronomia, Via Ranzani, 1, I-40127, Bologna, Italy

¹⁶ 16 Integral Science Data Centre, ch. d'Écogia 16, CH-1290 Versoix

¹⁷ 17 Geneva Observatory, ch. des Maillettes 51, CH-1290 Sauverny

¹⁸ 18 Università di Milano-Bicocca, Dipartimento di Fisica - Piazza delle Scienze, 3, I-20126 Milano, Italy

Received ...; accepted ...

Abstract.

In this paper we discuss the mix of star-forming and passive galaxies up to $z \sim 2$, based on the first epoch VIMOS-VLT Deep Survey (VVDS) data. In agreement with previous works we find that the global galaxy rest-frame color distribution follows a bimodal distribution at $z \leq 1$, and we establish that this bimodality holds up to $z \sim 2$. The details of the rest-frame color distribution depend however on redshift and on galaxy luminosity, with faint galaxies being bluer than the luminous ones over the whole redshift range covered by our data, and with galaxies becoming bluer as redshift increases. This blueing trend does not depend, to a first approximation, on galaxy luminosity. Using our spectroscopic dataset we can also separate galaxies based on a star-formation activity indicator derived combining the equivalent width of the [OII] emission line and the strength of the $D_n(4000)$ continuum break. The comparison between this spectral classification and the rest-frame colors shows that about 35-40% of the galaxies in the red sequence cannot be used to effectively isolate a sample of purely passively evolving objects within a cosmological survey. Connected to this result is also the finding that the color-magnitude relations derived for the color and for the spectroscopically selected early-type galaxies have remarkably similar properties, with the contaminating star-forming galaxies within the red sequence objects introducing no significant offset in the rest frame colors. Therefore the average color of the red objects does not appear to be a very sensitive indicator for measuring the evolution of the early-type galaxy population. Finally, we use the multi-band VVDS photometric data and spectral templates fitting to derive multi-color galaxy types, which have a slightly higher efficiency than rest-frame color in isolating the passive, non star-forming galaxies within the VVDS sample.

Key words. Galaxies: evolution - Galaxies: fundamental parameters - Galaxies: photometry

1. Introduction

Early-type galaxies are the preferred target for studies on how and when galaxies were formed, because of the simpler task of modeling an old stellar population undergoing passive evolution compared to modeling a young population continuously modified by an irregular star formation history. Over the last few years, mostly in response to the accumulating evidence in favor of a predominantly old stellar population within early type galaxies (see for a complete review Renzini 2006), the discussion has focused onto two main areas: the history of stellar formation and how and when stars assembled into galaxies. Still, a fundamental pre-requisite for such studies is to isolate from cosmological surveys a sample of early-type galaxies representative of the true galaxy population at all epochs probed.

Commonly used galaxy classification schemes are based purely on the morphological appearance of galaxies. It is well known however that galaxies follow a number of scaling relations involving their stellar populations and their morphological, structural and photometric parameters. Compared to their late-type counterparts, early-type galaxies have been found to be redder (color-morphological type relation, Roberts & Haynes 1994), more luminous (color-magnitude relation, Visvanathan & Sandage 1977; Tully et al. 1982), to be located in denser environments (morphology-density relation, Dressler 1980), and to have a star formation history that takes place over shorter time-scales (Sandage 1986; Gavazzi et al. 2002).

Cosmological survey studies, faced with the difficulty of obtaining a morphological classification for all the galaxies in their sample, have often tried to take advantage of those relations to define an alternate classification scheme. Galaxy color, which is by far the easiest parameter to measure for a full survey sample, has been most commonly used as a substitute for morphological information. Lately this practice has become even more commonplace, since the galaxy rest-frame color distributions have been found to be clearly bimodal. This bimodality was well known to exist within clusters of galaxies, where the early- and late-type galaxies follow two rather distinct color-magnitude relations, as discussed by Visvanathan & Sandage (1977) and Bower et al. (1992) for early-type galaxies and Tully et al. (1982) and Gavazzi et al. (1996) for late-type ones. That the same bimodality was present in a general field sample was first noticed in the local universe by Strateva et al. (2001) using the SDSS galaxies sample, and afterwards discussed by many other authors (see, as an example, Baldry et al. 2004a,b). Bell et al. (2004b) (hereafter B04) and Weiner et al. (2005) detected the rest-frame color bimodality also at higher redshifts up to $z \sim 1$, respectively in the COMBO-17 and DEEP data.

Color bimodality is interpreted as just one specific signature introduced by the general processes controlling galaxy formation and evolution (Menci et al. 2005; Dekel & Birnboim 2006). Other similar signatures are observed, since bimodality has been found to be a characteristic in the distribution of

many other observables like H_α emission (Balogh et al. 2004), 4000 Å break (Kauffmann et al. 2003b), star formation history (Brinchmann et al. 2004), or clustering (Budavári et al. 2003; Meneux et al. 2005).

Because of the age of their stellar population, early-type galaxies are expected to have very red optical colors over a rather large redshift range. This expectation has been confirmed in clusters of galaxies, where the red-sequence for morphologically selected early-type galaxies has been observed up to $z \sim 1.2$ (Kodama & Arimoto 1997; Stanford et al. 1998). As a result the red color has often been used as a tracer to isolate samples of early-type galaxies. Most recently the widespread acceptance of color bimodality has resulted in the use of red-sequence galaxies (those that populate the red peak of the color bimodal distribution) to study the evolution of early-type galaxies, implicitly assuming this red population to be entirely composed of old, passively evolving objects. One example of such a usage is provided by B04, who derive the luminosity function and therefore the luminosity density for the red galaxy population in the COMBO-17 survey, and then use this information to obtain an estimate of the growth of the stellar mass of early-type galaxies, assuming that the evolution of the luminosity density they derive is that of a purely passively evolving stellar population.

However, while most of the early-type galaxies are indeed red, they are possibly not the only red objects included in a survey sample. Attempts at quantifying the contamination of non early-type, passive objects within samples of red galaxies include both studies focused on Extremely Red Objects (EROs), and more general surveys which target the whole bulk of the galaxy population. Among EROs, Cimatti et al. (2002), using spectroscopic data for 45 objects, find a roughly equal proportion of early-type, passive galaxies and of dusty starburst objects. Among less extreme objects, in the local Universe Strateva et al. (2001) reported a significant fraction (20%) of galaxies morphologically later than Sa in the red galaxy population. This result is confirmed using the data for galaxies in the Virgo Cluster and in the Coma Supercluster provided by the GOLDMine database (Gavazzi et al. 2003). At intermediate redshift (up to $z \sim 1$) various studies are confirming these results (see for example Kodama et al. 1999; Bell et al. 2004a), while the nature of red galaxies at higher redshift is less clear. However, there are indications that the fraction of morphologically late-type galaxies with red colors could be even higher at $z \gtrsim 1$ (Strateva et al. 2001), in agreement with the findings based on EROs studies.

In this work we use VIMOS-VLT Deep Survey photometric and spectroscopic data (VVDS, see Le Fèvre et al. 2005) to compare the galaxy population that can be isolated by using either a red color selection criterion or a spectro-photometric classification. Although neither of these selection criteria can be considered entirely equivalent to a morphological classification in isolating a sample of early-type galaxies, our comparison does provide an estimate for the uncertainties involved in selecting those objects within a cosmological survey sample; this is a first step towards a better understanding of the uncertainties involved in galaxy formation and evolution studies. The paper is organized as follows. In section 2 we describe

* Based on data obtained with the European Southern Observatory Very Large Telescope, Paranal, Chile, program 070.A-9007(A), and on data obtained at the Canada-France-Hawaii Telescope, operated by the CNRS of France, CNRC in Canada and the University of Hawaii.

the VVDS galaxy sample and the data we use in this work. In section 3 we analyse the rest-frame color distributions and we demonstrate that the color bimodality is present up to $z \sim 2$. Then, in section 4, we study the color bimodality as a function of redshift and of galaxy luminosity. In section 5 we focus on the red-sequence galaxies studying their color-magnitude relation. In section 6, we analyse in detail the red-sequence objects showing how this population is contaminated by a non negligible fraction of starforming objects. We use the strong bimodality observed in the $\text{EW}([\text{OII}])\text{-}D_n(4000)$ distribution to isolate a sample of early-type galaxies less contaminated by star-forming galaxies than a simple color-magnitude selection. Finally in section 7 we discuss the color evolution of this sample.

All magnitudes are given in the Johnson-Kron-Cousin system; the adopted cosmology is the standard $\Omega_m = 0.3$, $\Omega_\Lambda = 0.7$ and $H_0 = 70$.

2. The Data

In this paper we focus exclusively on the VVDS-0226-04 field (hereafter F02), because within this field we have a very broad multi-wavelength coverage (from radio, far and near infrared, to optical, UV, and X-rays), and the F02 coverage at optical wavelengths is the deepest among the four VVDS fields, both photometrically and spectroscopically.

Our sample is selected from the first epoch VVDS-Deep spectroscopic sample within the F02 field (see Le Fèvre et al. 2005). This is derived from a purely magnitude limited sample, including all objects in the magnitude range $17.5 \leq I_{AB} \leq 24.0$ from a complete, deep photometric survey (Le Fèvre et al. 2004).

The whole 1.2 deg^2 field has been imaged in B, V, R and I with the wide-field 12K mosaic camera at the Canada-France-Hawaii Telescope (CFHT), reaching the limiting magnitudes of $B_{AB} \sim 26.5$, $V_{AB} \sim 26.2$, $R_{AB} \sim 25.9$, $I_{AB} \sim 25.0$. Data are complete and free from surface brightness selection effects down to $I_{AB} \leq 24.0$ (see for details McCracken et al. 2003). U-band data, taken with the Wide-Field Imager at the ESO/MPE 2.2m telescope, are available for a large fraction of the field, to the limiting magnitude of $U_{AB} \sim 25.4$ (Radovich et al. 2004). In all bands, apparent magnitudes have been measured using Kron-like elliptical apertures (the same in all bands), with a minimum Kron radius of 1.2 arcsec, and corrected for the Galactic extinction using the Schlegel dust maps (Schlegel et al. 1998).

Spectroscopic observations for about 23% of the objects included in the photometric magnitude limited sample have been carried out with the Visible Multi Object Spectrograph (VIMOS, see LeFevre et al. 2003), on the UT3 unit telescope of the ESO Very Large Telescope. The spectroscopic sample is close to be a perfectly random subset of the parent photometric sample, with only a small bias against large angular-size objects which is easily corrected for (see Ilbert et al. 2005; Bottini et al. 2005).

Spectra have been obtained during two observing runs between October and November 2002. All the data have been reduced with the VIMOS Interactive Pipeline and Graphical Interface software package (VIPGI, see Scodreggio et al. 2005;

Zanichelli et al. 2005). A redshift measurement has been derived for 9036 galaxies with a success rate which is mildly dependent on both the galaxy apparent magnitude and its redshift (see the discussion on the Spectroscopic Sampling Rate and Figures 2 and 3 in Ilbert et al. 2005). The median redshift for the whole spectroscopic sample is $z = 0.76$ (see Figure 25 in Le Fèvre et al. 2005).

The sample we use for this work is composed of all the galaxies with secure identification and redshift measurement (z quality flags 2,3,4,9 in Le Fèvre et al. 2005) in the F02 spectroscopic sample, with the restriction of having $z \leq 2.0$, in order to ensure that the observed optical and near-infrared magnitudes provide a reasonably close bracketing for the rest-frame optical magnitudes we use in our analysis. A total of 6291 galaxies are included in this sample with a measured B, V, R and I magnitude.

For all these objects we have obtained measurements of the equivalent width and line flux for all emission lines detected in their spectra, and also a measurement of the amplitude of the 4000 Å break, using the narrow break definition proposed by Balogh et al. (1999). All these measurements have been carried out using the PLATEFIT software package (Lamareille et al. 2006 in preparation), which implements the spectral features measurement techniques described by Tremonti et al. (2004). First, the best fitting stellar continuum taken from a grid of stellar population synthesis models generated using Bruzual & Charlot most recent synthesis code (Bruzual & Charlot 2003) is subtracted from the observed spectrum. After subtracting the best-fitting model, any remaining residuals in the continuum are removed by fitting a low order polynomial to it, and then all emission lines are fitted simultaneously with a Gaussian profile, imposing all the lines to have the same line-width and velocity offset, except for the unresolved $[\text{OII}]\lambda 3727$ doublet which is assumed to have a larger width. Finally, the results of the fit are used to remove the emission lines from the observed spectrum, before measuring stellar continuum or absorption features.

In this work we use measurements of the $[\text{OII}]\lambda 3727$ line equivalent width and of the 4000 Å break (D4000). Because of the wavelength coverage of the VVDS spectroscopic observations, these measurements are possible only for objects in the redshift range $0.45 < z < 1.2$; 4433 objects are included in this spectroscopic sub-sample. Approximately half of these (2229 objects) are part of the high signal-to-noise spectra sub-sample used in section 6 to investigate the effects of data quality on the spectral measurements, and therefore on the reliability of our analysis.

3. Rest-frame colors and color bimodality

Rest-frame colors for all galaxies in the sample are computed from the absolute magnitude estimates derived as described in Appendix A of Ilbert et al. (2005). For a given rest-frame photometric band and a given galaxy redshift, the absolute magnitude is obtained from the apparent magnitude measurement within the observed photometric band that most closely matches the rest-frame one. A k -correction is then applied to take into account the residual difference between the two pho-

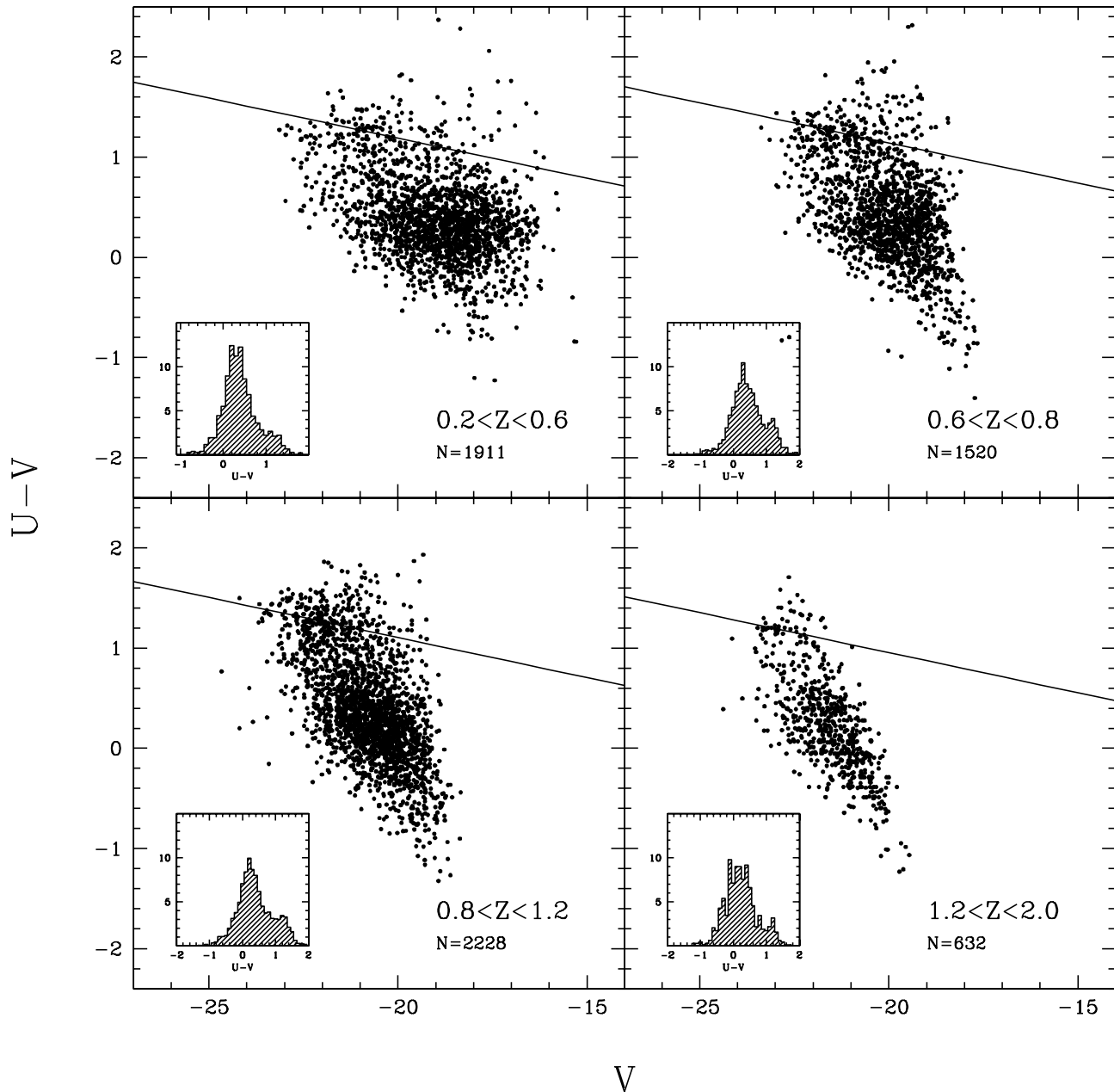


Fig. 1. The rest-frame U-V color against the absolute V magnitude for our sample in four different redshift intervals. The inset in each panel shows the corresponding color distribution, i.e. the projection of the color-magnitude on the U-V axis. The solid line is the fit of the red sequence (see paragraph 5).

tometric bands. The amplitude of the k-correction is derived by selecting the best-fitting galaxy spectra template to the galaxy B, V, R, I magnitude measurements.

In this work we focus on the rest-frame U-V color, mainly because it allows us to sample the amplitude of the 4000 Å break in the Spectral Energy Distribution, which is a good indicator of the galaxy stellar population age (Bruzual 1983; Kauffmann et al. 2003a). Another advantage provided by this choice of rest-frame photometric bands is that they are bracketed by the observed bands for most of the redshift range cov-

ered by our sample. As discussed in Ilbert et al. (2005), typical k-correction uncertainties are of the order of 0.04 mag for the U-band, and of 0.11 mag for the V-band. When these uncertainties are added to the apparent magnitude measurement one (approximately 0.1 mag for the faintest object), they contribute to a total color measurement uncertainty of up to 0.2 mag. Finally, U-V is a color often used by previous works on the properties of early-type galaxies, both locally (for example Visvanathan & Sandage 1977; Bower et al. 1992) and at redshifts up to 1 (see B04).

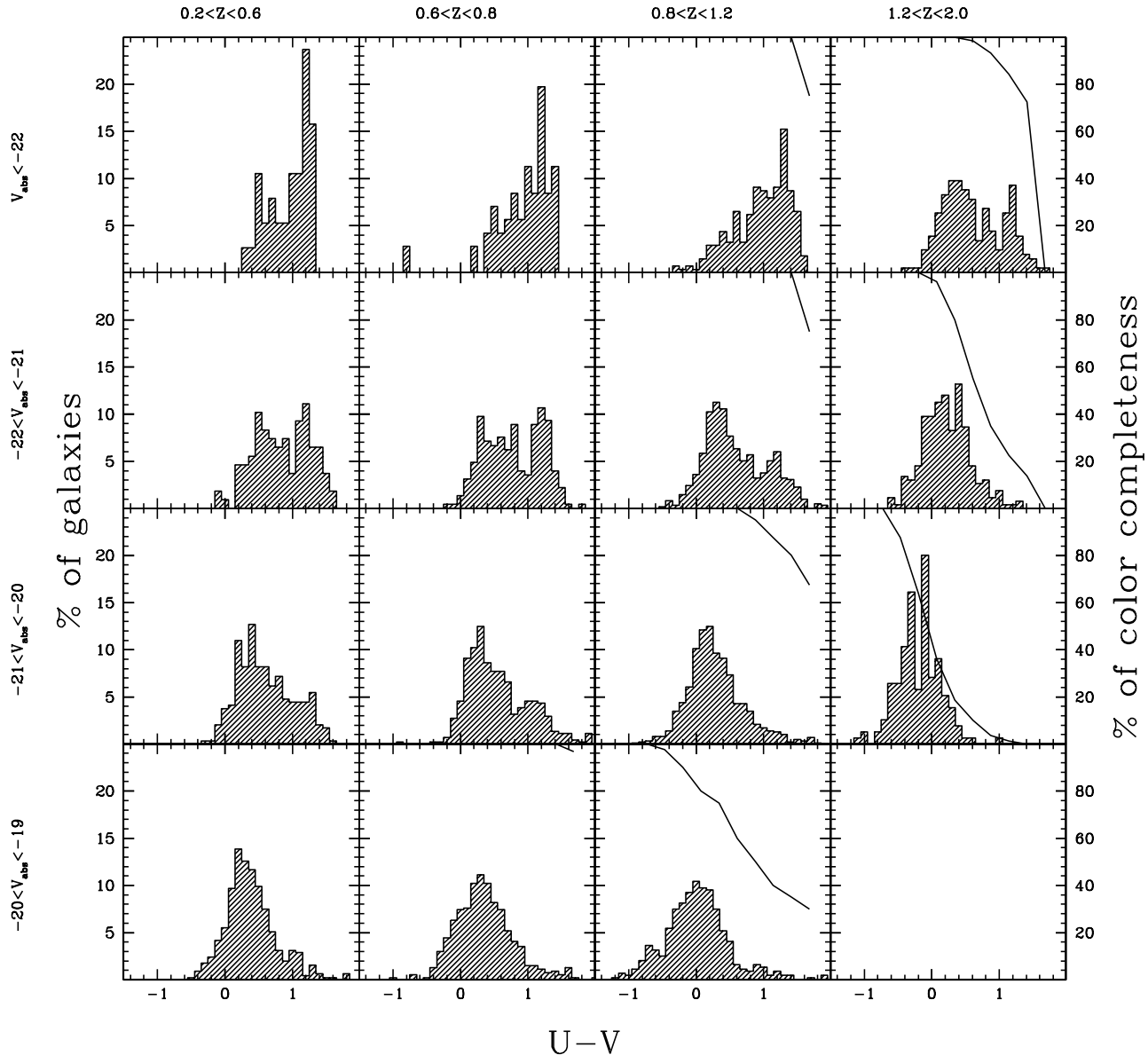


Fig. 2. The U-V rest-frame color distributions divided in absolute magnitude and redshift bins; luminosity increases from bottom to top, redshift from left to right. The histograms scale is shown on the left side of the plot. The solid line plotted in some bins highlights the color regions which are “forbidden” by the VVDS selection criteria (see the text for details); the scale of these lines is shown on the right side of the plot.

The distribution of the rest-frame U-V color against the absolute V magnitude for our sample is shown in figure 1, over four different redshift intervals. The small inset in each panel shows the corresponding color distribution, i.e. the projection of the color-magnitude on the U-V axis. In agreement with previous SDSS (Strateva et al. 2001), DEEP (Weiner et al. 2005) and COMBO-17 (B04) findings, a bimodal color distribution is observed. Moreover the depth of our sample is allowing us to extend the detection of such a bimodality up to at least $z = 1.5$

(the mean redshift for the galaxies in the highest redshift bin). This is in good agreement with the galaxy formation model discussed recently by Menci et al. (2005), who predict a color bimodality to be clearly present up to $z \approx 1.5$ (see their figure 4), as a result of the interplay between the merging histories of forming galaxies and the feedback/star formation process. Within such a hierarchical clustering scenario, the star formation histories of massive galaxies and those of galaxies formed in biased, high density regions are generally peaked at higher

redshift compared to those of less massive galaxies or galaxies formed in low density environments. As a result, the color bimodality is expected to originate at redshift $z \approx 4 - 5$, although it might be very difficult to observe it at $z > 2$, given the typical accuracy with which rest-frame colors are derived.

We also remark that within our data the bimodality is visible irrespective of the detailed choice of filters that one could use to define the rest-frame color: we observe a rather similar bimodal distribution using any combination of the U, B, V, R, and I filters.

4. Rest-frame colors and galaxy luminosity

The insight that the bimodal color distributions discussed above provides into galaxy formation and evolution processes is however limited. It is well known that both early- and late-type galaxies follow some form of color-magnitude relation, although the two relations are quite different from each other; see, for example, Visvanathan & Sandage (1977) and Bower et al. (1992) for early-type galaxies and Tully et al. (1982) and Gavazzi et al. (1996) for spiral galaxies. This fact alone has certainly an impact on how the red and blue components in the color distribution presented above are populated. Equally important in this respect is the role of the environment, driven by the density-morphology relation, and the work of Baldry et al. (2004b) on the SDSS sample illustrates the gradual change in the proportion of blue and red galaxies as a bivariate function of galaxy luminosity and local density. Cucciati et al. (2006) have obtained similar results on the VVDS data.

The influence that luminosity has on the proportion of red and blue galaxies is particularly important in our study, because of the large redshift interval covered by our sample. We present in figure 2 the rest-frame color distribution divided both in redshift and in absolute magnitude bins.

Within the VVDS, as in all magnitude limited surveys, the range of luminosities covered by the sample changes with redshift, moving towards higher luminosities with increasing z . As the apparent magnitude for a galaxy in a given photometric band depends on its luminosity, redshift, and spectral energy distribution (and therefore its color), it is expected that, for a given redshift and luminosity, galaxies with rest-frame color above a certain value should be systematically excluded from the sample, simply because their apparent I-band magnitude becomes too faint, while bluer galaxies with the same luminosity are still above the limiting magnitude because of their flatter spectrum (see Ilbert et al. 2004). To quantify how this selection effect might bias our results we have derived a rest-frame color vs. apparent I-band magnitude relation for the galaxies within each redshift and absolute magnitude bin in figure 2 using synthetic spectral energy distributions (SED). These were obtained using publicly available stellar population synthesis models from Bruzual & Charlot (Bruzual & Charlot 2003), which provide the time evolution of a galaxy stellar spectrum as a function of galaxy age, star formation history and stellar initial mass function. For this work we have always used a Salpeter initial mass function (Salpeter 1955). For the star formation history (SFH) we follow Gavazzi et al. (2002) in using a slightly more realistic set of SFHs with respect to the com-

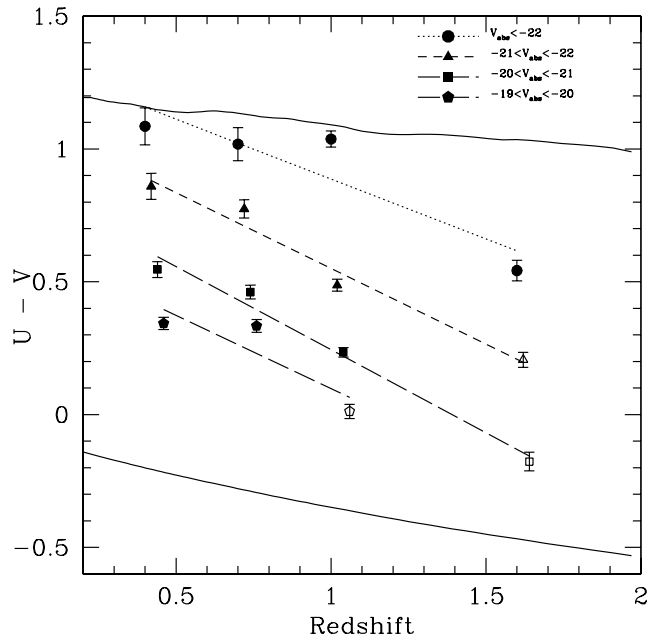


Fig. 3. The median color values for the redshift and luminosity bins from figure 2. Open symbols indicate the bins where the color distribution is affected by the sample selection effect discussed in the text. Error bars represent the statistical error in the median value determination. The dashed lines are linear fit to the data in the various bins. For comparison, the two curves represent the color evolution of the template which, in our grid, better approximates a constant SFH (bottom line) and a Single Stellar Population (top line).

monly used exponentially decreasing one. To cover as wide a range of galaxy properties as possible, we generated a wide grid of model parameters and derived a synthetic SED for each grid point. All ages from 0 to 20 Gyr and all star formation time-scales from 0.1 to 25 Gyr are covered by the grid.

Because of the non negligible ranges of redshift and luminosity spanned by each of our figure 2 panels, we have subdivided each panel into 10 intervals, thus obtaining a grid of 100 redshift-absolute magnitude combinations. For each couple of values our set of synthetic SEDs has been redshifted and scaled and the apparent I-band magnitudes and rest-frame U-V colors have been computed for each SED of the set. The SEDs producing apparent I-band magnitudes brighter than the VVDS sample selection limit are considered as observable by the VVDS, and sorting them by their color we derive an estimate of the reddest galaxy color still potentially observable in the VVDS sample for any given redshift-luminosity combination. We therefore derive an estimate of the color bias within each figure 2 panel by counting the fraction of redshift-luminosity grid points for which a given color is bluer than the corresponding reddest color potentially observable. This simple computation is equivalent to assuming a uniform luminosity and redshift distribution for the objects within the given panel limits. That is not the case for the real sample, but in practice the larger fraction of fainter objects (less likely to be observable above the apparent magnitude limit) is compensated quite

effectively by a larger fraction of objects on the lower redshift half of the bin (which are more likely to be observable).

Whenever this fraction of redshift-luminosity grid points is below 100%, it is plotted as a thick line in figure 2. When this percentage is too low (say $\lesssim 50\%$) the corresponding color is clearly biased against in our sample, and therefore the color distribution plotted for the given redshift and luminosity bin might not be representative of the whole galaxy population within the bin boundaries. We see from figure 2 that the color completeness is good with the exception of the highest redshift/lowest luminosity bins. It is evident that a global color-magnitude relation, with galaxies becoming redder as their luminosity increases, is present over the whole $0 < z < 2$ redshift interval. At the same time we also notice how, within a fixed luminosity bin, galaxies become bluer with increasing redshift, and this effect is present at all luminosities covered by our sample. This result is in agreement with the findings of previous redshift surveys like the CFRS (Lilly et al. 1995) and the Hawaii Deep Fields Survey (Cowie et al. 1996), but it is the first time that this findings are extended significantly over the $z \approx 1$ limit. The discussion in the previous paragraph on the color selection bias shows that these trends are not artificially created by the VVDS sample definition.

In figure 3 the median values of each color distribution are plotted, for the same luminosity bins used in figure 2. The two effects discussed in the previous paragraph are quite clearly visible. The blueing of galaxies as redshift increases is quite independent from the absolute magnitude. A possible exception is presented by the most luminous objects, for which the global blueing is driven by the last point only. For comparison, we have plotted the color evolution of two synthetic SEDs extracted from the grid we have used to determine the selection bias. The models are the one which better approximates a constant SFH (bottom line) and the passive evolution of a Single Stellar Population (top line).

5. The color-magnitude relation of the red galaxies

Table 1. The red-sequence CMR intercept

Redshift	N_{galaxies}	$(U - V)_{M_V = -20}$	σ
0.2 - 0.4	82	1.308	0.314
0.4 - 0.6	123	1.218	0.254
0.6 - 0.8	259	1.204	0.290
0.8 - 1.0	229	1.179	0.209
1.0 - 1.2	133	1.161	0.178
1.2 - 1.4	44	1.047	0.253
1.4 - 2.0	17	1.005	0.078

The properties of the color-magnitude relation (CMR) of early-type galaxies (scatter, slope, and evolution with redshift) have often been used to constrain formation and evolution scenarios for this galaxy population (see for example Bower et al. 1992; Kodama & Arimoto 1997; Bernardi et al. 2003). These

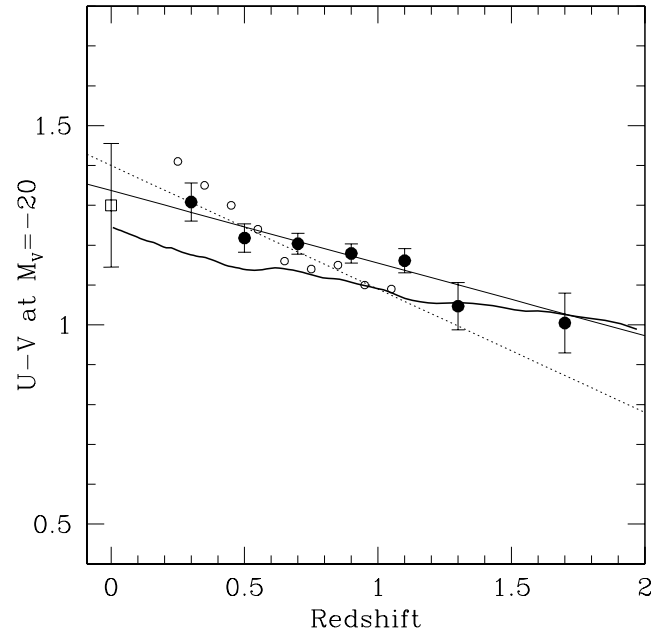


Fig. 4. Color evolution of the red sequence as measured by the value of the intercept of the CMR at $M_V = -20$. Small open circles and the dotted line are from B04; large filled circles and the solid line represent our VVDS data and the best linear fit to them. The open square point at $z = 0$ is the $U - V$ CMR zero point at $z = 0$ computed by B04 from SDSS data. The thick solid curve is the color evolution of the template which, in our grid, better approximates a Single Stellar Population. Error bars account only for the statistical uncertainties in the CMR zero-point determination

studies were mostly based on cluster samples of morphologically defined early-type galaxies, and it was not entirely obvious how a similar kind of analysis could be performed on a sample of color-selected objects in a large survey lacking the necessary high resolution imaging to perform the appropriate morphological classification.

B04 have demonstrated that with a large sample and good photometric redshift estimates like those provided by the COMBO-17 survey, such kind of analysis is possible. Here we follow their procedure to study the redshift evolution of the CMR in the VVDS sample, while in section 7 we try to quantify the effect on this evolution produced by a significant contamination of the red color-selected galaxy population by star-forming galaxies (see section 6).

Following B04, we have estimated the zero-point of the CMR constraining the slope to assume the value which has been determined for local galaxy clusters (-0.08 , see Bower et al. 1992). The bi-weight mean corrected color of all red galaxies with rest-frame color $U - V > 1$ is determined after having removed the fixed CMR slope from the individual measurements. The solid line plotted in each panel of figure 1 shows the corresponding fit of the red sequence in the respective redshift range.

Figure 4 shows the value of the fitted CMR intercept at $M_V = -20$ as a function of redshift; plotted values are summarized in Table 1. The evolution of this population is quite

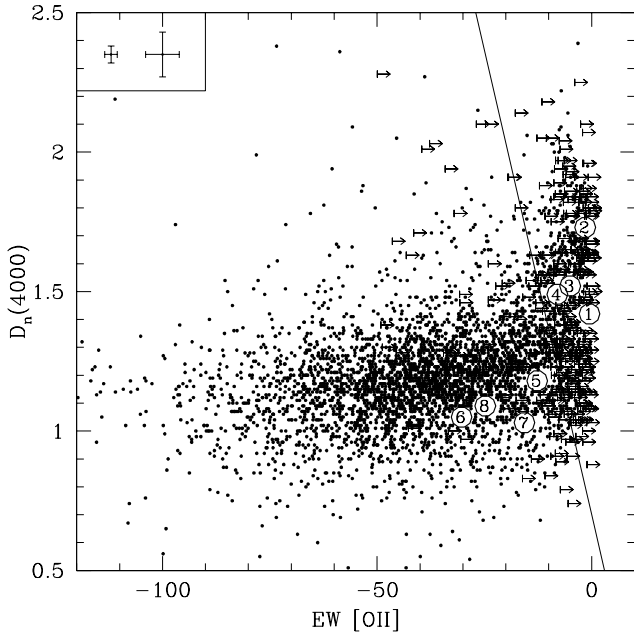


Fig. 5. The $D_n(4000)$ distribution as a function of the rest frame $EW([OII])$. Only 2σ or higher confidence $D_n(4000)$ measurements are plotted. For $EW([OII])$ measurements with a confidence level lower than 2σ upper limits are plotted. The error bars in the upper left corner of the plot show the typical measurement uncertainties for the higher S/N spectra (left) and the lower S/N spectra (right) sub-samples. The solid line divides the sample in the passive population (ET) and star-forming population (LT). For comparison the large numbered circles are the $D_n(4000) / EW([OII])$ values for the Virgo cluster templates from Gavazzi et al. (2002) as listed in Table 2

visible; from $z \sim 0.3$ to $z \sim 1.7$ red galaxies become bluer by ~ 0.3 mag. The solid line is a linear fit to the evolution: $U - V = 1.355 - 0.206 \times z$. The results of B04 on the COMBO-17 data are plotted for comparison; also the $U - V$ CMR zero point at $z = 0$ determined by B04 from SDSS data is shown. Our results qualitatively confirm the evolution claimed by B04 and extend it up to $z \sim 2$. However we find that the amount of this evolution, quantified by the slope of the relation, is somewhat lower than reported by B04, and this result is bringing the whole evolutionary trend in better agreement with the $z = 0$ SDSS-based point. The thick line plotted in figure 4 shows the color evolution of the synthetic SED within our models grid which better approximates a Single Stellar Population. As already noticed by B04, there is a general good agreement between the observed evolution of the CMR and the expectations for a purely passively evolving population. Our results show that this agreement extends at least up to $z \sim 2$.

6. The nature of the red population: separating star-forming from passively evolving galaxies

In this section we intend to quantify how the contamination from late-type, star forming galaxies is affecting the properties of the red color-selected population, and how this effect is changing with redshift. We use the VVDS spectroscopic infor-

Table 2. The $D_n(4000)$ and rest-frame $EW([OII])$ values for the Virgo templates plotted in figure 5

Label	Type	$D_n(4000)$	$EW([OII])(\text{\AA})$
1	dE	1.42	< 0.5
2	E/S0	1.73	< 0.5
3	Sa	1.52	< 5.0
4	Sb	1.49	< 8.0
5	Sc	1.18	-12.69
6	Sd	1.05	-30.31
7	Irr	1.03	-15.66
8	BCD	1.09	-24.79

mation to separate our sample into two classes of old, passively evolving and of young, star-forming objects. In figure 5 the relation between the equivalent width of the $[OII]\lambda 3727$ line ($EW([OII])$) and the 4000 \AA break ($D4000$) for the VVDS subsample for which these measurements are available is shown. This subsample is restricted to the redshift range $0.45 < z < 1.2$; outside these limits the VVDS observational set-up is preventing the measurement of these spectral features (see Le Fèvre et al. 2005). All the analysis done in the following sections is therefore limited to this range.

It is clearly visible from the plot how objects follow an L-shaped distribution, with most of the star-forming objects that have a large $EW([OII])$ having a negligible $D4000$, and vice-versa most of the objects that have a strong $D4000$ showing no significant $[OII]$ emission in their spectra. This suggests a natural sub-division of the galaxy population into two classes. We define *spectral early-type* objects (ET) galaxies in the vertical arm of the two parameters distribution, i.e. those that do not show any detectable sign of star formation activity, and which can be expected to undergo further evolution only via passive evolution of their stellar population. Conversely, we define *spectral late-type* objects (LT) galaxies in the horizontal arm, still undergoing a vigorous star formation activity. More elaborated spectral classification schemes have been proposed in the past, like the four-fold subdivision discussed by Mignoli et al. (2005), but we prefer to use here a simpler two-fold subdivision, that mirrors the one obtained using the rest-frame colors.

To a first approximation the exact definition of the separating boundary between LT and ET galaxies in the $D4000$ vs. $EW([OII])$ parameters space could be a vertical line at $EW([OII]) = 10 \text{\AA}$, the approximate detection limit for the $[OII]$ line in our data. This definition, however, would lead us to include many objects with very low $D4000$ and a real, albeit undetected, $[OII]$ emission in the ET sample, which is obviously contrary to the natural definition of early-type galaxies as objects with an old stellar population (large $D4000$) and no current star formation activity (no $[OII]$ emission line). To alleviate this problem, we have built a composite spectrum of the ET population for various slopes of the separating boundary line. Then we have selected the subdivision that minimizes the equivalent width of the $[OII]$ line in the composite spectrum of the resulting ET population. This optimization

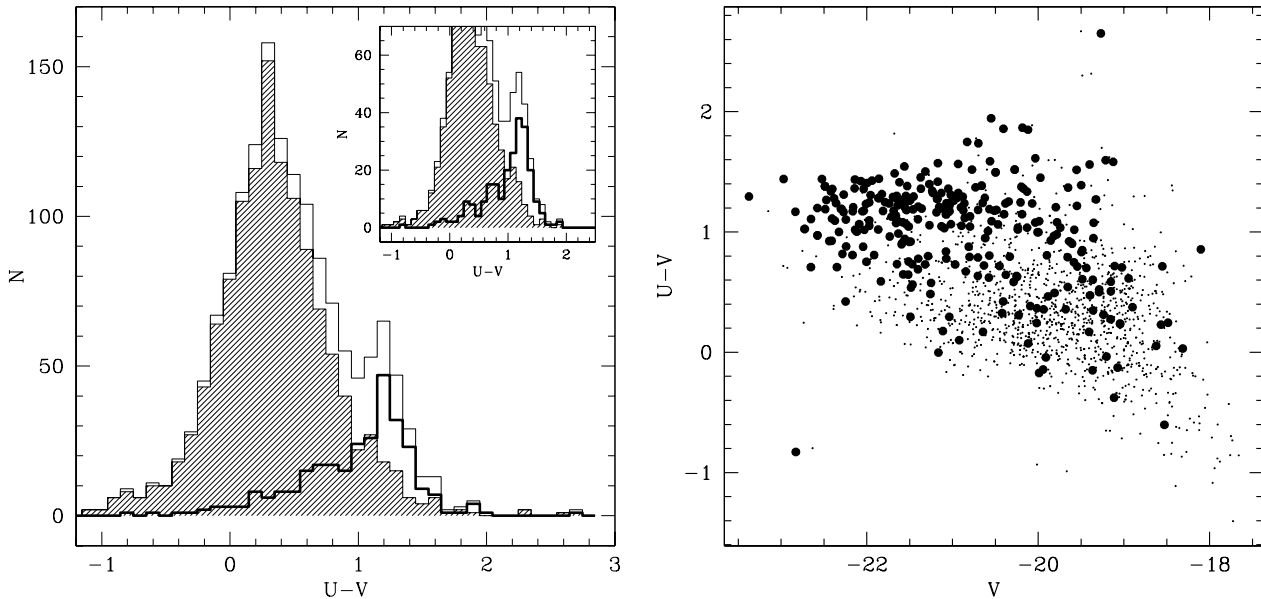


Fig. 6. **a)** U-V rest-frame color distribution; the shaded histogram is for the LT population, while the heavy line histogram is for the ET population. The inset shows the same histograms drawn only for the higher S/N objects. **b)** U-V vs V color-magnitude relation ; big black dots are ET objects, tiny dots are LT ones. Both plots include only the objects with redshift within the interval 0.6-0.8.

procedure results in a slightly tilted boundary line described by the relation:

$$D_n(4000) + EW([OII])/15.0 = 0.7$$

ET galaxies have $D_n(4000) + EW([OII])/15.0$ above 0.7, while LT galaxies are below that value. For comparison, in figure 5 we have also plotted as large numbered circles the $D_n(4000)$ and $EW([OII])$ values measured on Virgo cluster templates from Gavazzi et al. (2002). Table 2 recaps the legend for the circles. It should not be surprising that our ET-LT boundary is including early spirals within the ET population, and only Sc and later types within the LT population. This is a rather general property of classification schemes based on galaxy color or spectral properties. For example, the earliest spiral galaxy SED presented by Coleman et al. (1980) is that typical of Sbc galaxies, and this same SED was used by Lilly et al. (1995) to separate red and blue galaxies in their CFRS galaxy sample; the earliest spiral galaxy color-color track used by Adelberger et al. (2004) in defining the color selection criteria for isolating star-forming galaxies in the redshift range $1 < z < 3$ is that typical of an Sb galaxy.

We consider this spectral classification as a better substitute for a true morphological classification in respect to color for a number of reasons: it is based on directly measurable quantities and avoids the uncertainties involved in estimating rest-frame colors; it provides a rather direct measurement for the age of the stellar population and the amount of star formation activity taking place in each galaxy; unlike colors, it is minimally affected by the unknown amount of reddening inside each galaxy. One possible limitation affecting our spectral classification is the fact that a number of objects with relatively young stellar

population, as witnessed by the small value of their D4000, is included within the ET population. However we prefer not to exclude these objects by some modification of the ET-LT separation boundary, because any such a modification would make our classification scheme much more vulnerable to progenitor bias effects. With the current scheme as soon as a galaxy has completed the bulk of its star formation activity and is starting the purely passive evolution phase it becomes an ET object, and it remains one at all subsequent times, as its stellar population ages and the D4000 amplitude in its spectrum increases. Instead any significant star formation activity would move an object towards the left in the figure 5 diagram, effectively removing it from the ET population. This minimization of progenitor bias effects on our classification scheme is the main reason we can use a redshift-independent classification scheme in our analysis.

Having obtained an early- vs. late-type galaxy separation based on spectral properties, we analyse what is the color distribution of these two categories, and compare this spectral classification with the “red-peak” color one. Figure 6a shows the global U-V rest-frame color distribution for our sample in the redshift interval where the peak of the $N(z)$ distribution is located ($0.6 < z < 0.8$, see Le Fèvre et al. 2005). The shaded histogram represents the color distribution for the LT objects, while the thick line shows the distribution for the ET population. The thin line histogram represents the sum of the two distributions. As expected, the red peak of the global color distribution is mainly populated by ET objects, while the blue peak is mainly populated by LT ones, but a rather strong contamination between the two populations is present. In fact, the color distributions for the two populations have a very significant overlap at intermediate colors, and a simple color cut is not

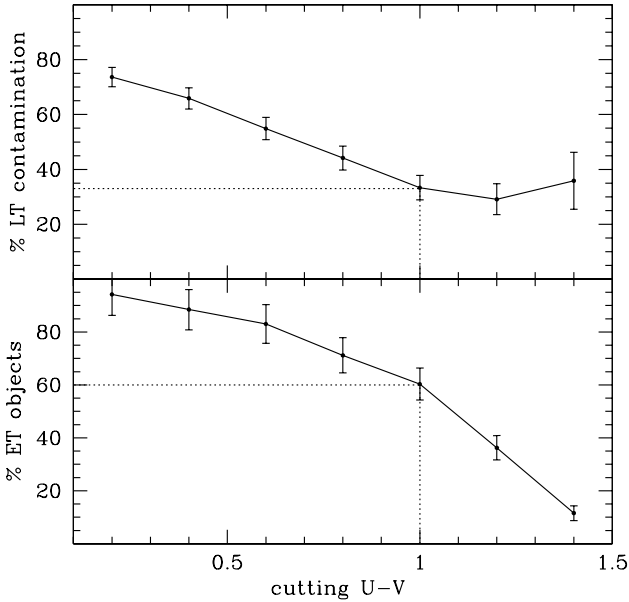


Fig. 7. The “contamination” effect in the redshift range $0.6 < z < 0.8$. The fraction of the whole ET population which is included in the resulting RED population (lower panel) and the “contamination” of the resulting RED sample (upper panel) as a function of the limiting color used to define it.

able to separate the galaxy populations according to the spectral classification defined above. Therefore it is not able to separate them on the basis of their stellar population and star formation history properties. The inset plotted in figure 6a shows the same histograms drawn considering only the objects with higher S/N spectra; it is easy to see how very little difference is observed when removing low S/N spectra objects, for which spectral feature measurements are more uncertain. We therefore conclude that uncertainties in the spectral classification are not the primary source for the significant overlap in color space between the two populations.

Similar results have been obtained by Bundy et al. (2005) using the DEEP2 data (see their figure 1), although they use a different color and a slightly different criterion for their spectral classification of passive and star-forming galaxies. The same contamination effect is visible in the full color-magnitude relation plot (figure 6b). Projecting the color-magnitude relation along the slope of the red sequence to obtain “corrected” color histograms, as done for example in B04, does not significantly change the situation.

6.1. Quantifying the contamination

From the total histogram in figure 6 we see that a purely color-based definition of the red peak population would be that of galaxies with $U - V > 1.0$, in agreement with the color cut implemented by B04. This is the color where a local minimum is observed in the color distribution, and it is also the color at which we observe the transition from an LT dominated population to an ET dominated one. However, because of the signifi-

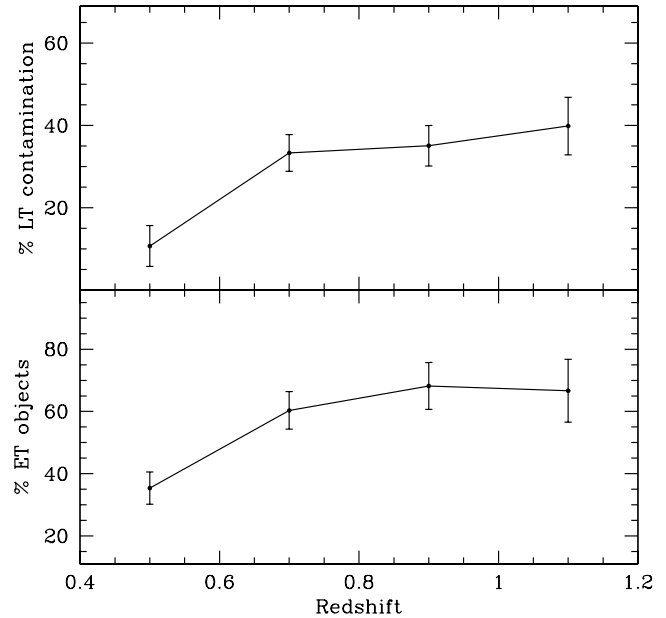


Fig. 8. The fraction of the ET objects which are included in the RED population and the corresponding LT contamination computed for a limiting color $U - V = 1.0$ as a function of redshift.

cant color overlap between the two populations, it is clear that the resulting RED population includes not only ET (i.e. really passive) objects, but also a significant fraction of LT (i.e. star-forming) ones. Moreover this RED population does not include a significant fraction of ET objects which have bluer colors.

In figure 7 we quantify this “contamination” (again in the redshift range $0.6 < z < 0.8$). The lower panel shows, as a function of the color cut we use to define the RED population, the fraction of the whole ET population which is included in it. The upper panel shows, on the contrary, the “contamination” of the resulting RED sample, i.e. which percentage of the total RED population is composed of LT objects.

Error bars in this and the following 2 figures have been computed using simple Montecarlo simulations. The main sources of uncertainty, beside the Poissonian error on population counts, are the uncertainties on the spectroscopic and photometric measurements. In our simulations we generated mock datasets by adding to the measured values random offsets, generated from a Gaussian distribution characterized by a σ equal to the measurement uncertainty for the given quantity. Then we repeated our determinations of the contamination effect for all the mock datasets to obtain an estimate for standard deviation of each data point in the plots.

To these Montecarlo uncertainty estimates we have also added the appropriate Poissonian counting uncertainties. The small values for the contamination uncertainties demonstrate that the effect we are witnessing is real, and not the result of some bias introduced by measurement uncertainties. Using the $U - V > 1.0$ cut we include in the RED population only $\sim 60\%$ of the ET objects, the remaining $\sim 40\%$ having bluer colors. At the same time, 35% of our RED population will be actually

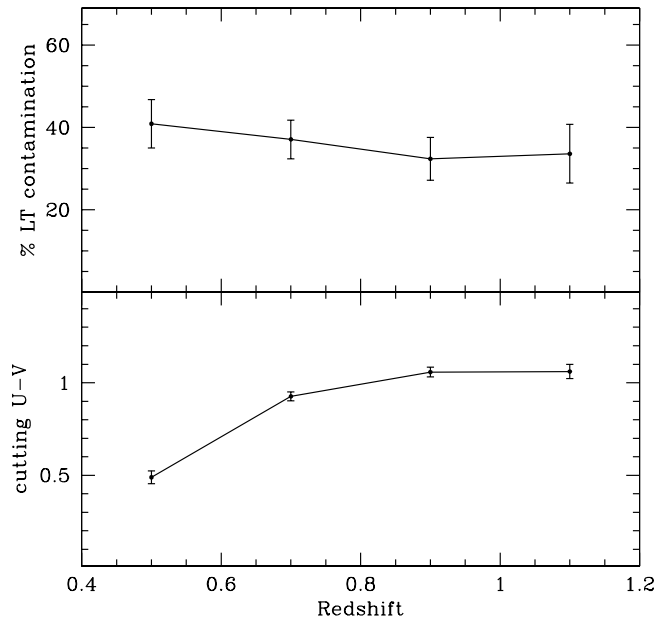


Fig. 9. The limiting $U-V$ color and the corresponding LT contamination of the RED population for a fixed fraction of ET object included in the resulting RED population (65%).

constituted by LT objects which have red colors, but show clear spectroscopic indication of star forming activity.

To summarize, 65% of our RED population will be ET population (and these objects are 60% of all the ET objects) while 35% will be LT objects.

These numbers change somewhat with redshift. By fixing the RED cut color at $U-V > 1.0$ we can follow how the fraction of the ET objects which are included in the RED population and the corresponding LT contamination evolve with redshift. This is shown in figure 8. If we use this “fixed color” approach the fraction of ET included objects and the corresponding LT contamination shows very little evolution over most of the redshift range we cover with our sample. The exception is represented by the lowermost redshift bin, but this is significantly affected by the sample characteristics. The VVDS has a relatively small field of view and therefore the number of bright objects we have in the lowest redshift bins is very small. Therefore the VVDS sample is by construction somewhat depleted of bright objects at low redshift, and since these bright objects are predominantly red galaxies, this results in both a smaller fraction of ET galaxies included in the red sample, and also in a smaller contamination of LT galaxies.

Using a slightly different approach, we fix the fraction of ET object we want to include in the resulting RED population and follow how the cutting color (and again the corresponding LT contamination) changes with redshift. This is shown in figure 9 for a fixed fraction of 65%. In this “fixed fraction” approach the fraction of ET included objects is fixed (by definition), the cutting color evolves up to $z \sim 0.6$ and then remains stable at $U-V \sim 1$, while the LT contamination evolves mildly with redshift. Once again, this redshift evolution is significantly affected by the sample properties discussed above.

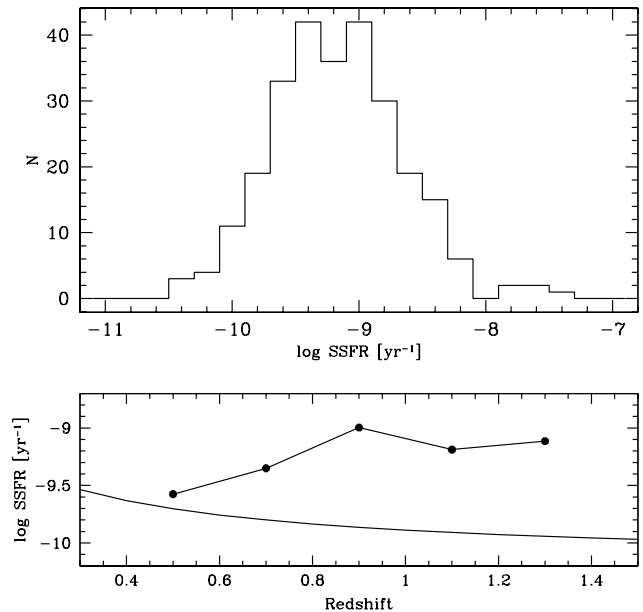


Fig. 10. In the upper panel the distribution of star formation rates for the contaminating LT population among the RED galaxies is shown. The evolution of the median value with redshift is plotted in the lower panel. The solid line is the SSFR which is required to double the galaxy stellar mass between the given redshift and the present time, which discriminates between quiescent and strongly star-forming galaxies.

Both approaches show how, using a fixed color cut at $U-V \sim 1$ at each redshift, we are not analyzing a real “passive” population, but the contamination (at least for $z \gtrsim 0.6$) is quite constant. To quantify how far away from a passively evolving object is the typical contaminant galaxy, we have derived current specific star formation rate estimates for all the RED population LT galaxies, using the [OII] luminosity conversion factor given by Kennicutt (1998). The resulting distribution of specific star formation rates is shown in the upper panel of figure 10 and has a median value of $10^{-9.17} \text{ yr}^{-1}$. The lower panel of figure 10 shows the evolution of the median value with redshift. The solid line represents the SSFR which is required to double the galaxy stellar mass between the given redshift and the present time, assuming a constant SFR; this “doubling” SSFR is used to discriminate between quiescent and star-forming galaxies. It is easy to see that, at all redshifts, the median SSFR value is above the threshold. It is clear that a significant number of dusty starbursting galaxies is included in the RED population, and its presence should be accounted for in studying the evolution of the RED population properties. This result is in agreement with the findings of Giallongo et al. (2005), who found some 35% of dusty starburst objects within the red population of their HDF N+S sample, and with those of Cassata et al. (2006), who found a fraction of 33% edge-on spirals within their sample of red galaxies in the COSMOS survey field.

Finally, we must remark that the type mix in the RED population depends on the range of galaxy luminosities that are

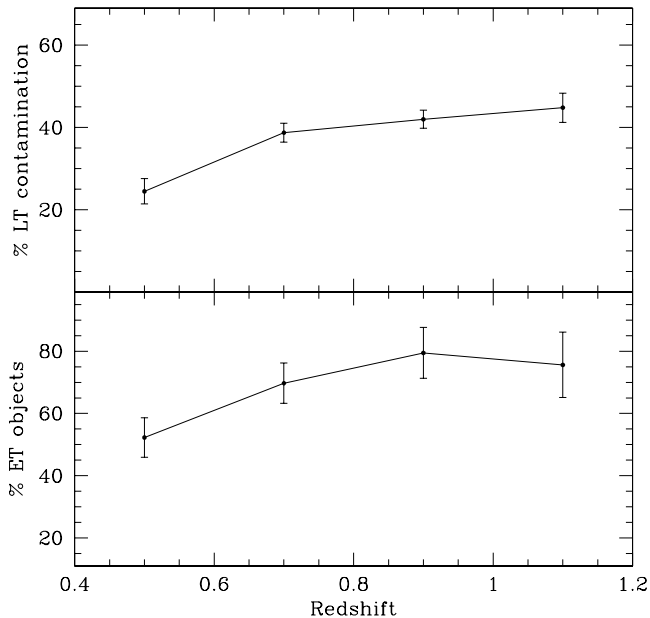


Fig. 11. The fraction of the ET objects which are included in the RED population and the corresponding LT contamination computed for multi-color types (see section 6.2)

included in the sample, in agreement with the model predictions discussed by Kaviraj et al. (2006). The fraction of ET galaxies included and that of LT galaxies contaminants among the RED population change from 60 and 35 percent respectively when the whole VVDS sample is considered, to 70 and 20 percent when only objects brighter than $M_B = -21$ are considered. Although a small part of this change could be due to larger errors in the measurements of photometric and spectroscopic parameters for the fainter objects, we clearly observe that transition objects (blue ET or red LT galaxies) are found preferentially at fainter luminosities.

6.2. The multi-color type approach

Given the not entirely satisfactory results obtained by a pure color selection in isolating an old, passively evolving galaxy population, we have considered also an alternative approach towards this goal, still based solely on photometric data. As described in Zucca et al. (2005), we are fitting the available optical photometry data with local spectral templates taken from Coleman et al. (1980), supplemented with two starburst templates, to derive a photometric type for each galaxy in our sample. Here we are considering the E/S0 and the early spiral photometric type objects together as a photometric early-type population, and the late-type spiral, irregular and starburst photometric type objects together as a photometric late-type population.

Our approach does not account for any global SED variation over cosmic time as a result of the evolution of the stellar populations, nor for the effects of a progenitor bias (van Dokkum & Franx 2001) against the early-type galaxy population. Still, it provides a very simple and model-independent

“no evolution” reference for any other, more complex modeling of galaxy populations evolution. Moreover, by comparing figure 8 with figure 11 we see that even though we do not account for evolving SEDs, the multi-color type approach has a relatively higher efficiency in separating old passive galaxies from star forming ones. Indeed with the single color separation we isolate on average (over the redshift range covered by our sample) about 60% of the ET galaxies, whereas in the case of the multi-color separation this fraction is 70%. We note that the 35% level of LT contamination is similar in both cases. Also the trends with redshift of both the fractions of selected ET galaxies and of LT galaxies contamination are comparable to the single color approach, since in both cases the selection criterion does not evolve with redshift.

Given the above results, we conclude that the photometric types approach is to be preferred to the color selection one, as it provides a finer degree of subdivision between galaxy properties than the color separation, making it a better tool for the study of galaxy evolution. Again, like in the case of the color selection, we observe a luminosity dependence for the population mix. Limiting our sample to the bright $M_B < -21$ objects we find that the photometric type criterion isolates 80% of the ET galaxies, with a contamination from LT objects reduced to 25%.

7. The CMR of the spectral early-type population

In section 5 we have analyzed the properties of the CMR of color-selected early-type galaxies in our sample, showing that there is a general good agreement between the observed evolution of the CMR and the expectations for a purely passively evolving population. In the following paragraphs, however, we have shown how this agreement is in fact a rather fortuitous one, because of the very significant contamination of the red population from (presumably dust-reddened) actively star-forming galaxies.

In figure 12 we now plot the evolution of the CMR for the spectroscopically selected ET galaxies (filled squares), and also for the multi-color selected early-type ones (open triangles). From a comparison with figure 4 we can see that only small changes are present in the CMR of the different early-type samples (the solid circles in this figure are the same as in figure 4, representing the evolution of the CMR for the color-selected red galaxies). The color-magnitude relations of ET and multi-color selected early-type galaxies are on average 0.15 magnitudes bluer than that of red galaxies, as could be expected from the presence of a blue color tail in these galaxy samples. As already noticed in section 6.1, the ET galaxies color distribution within the lowermost redshift interval is abnormally blue, and this is mirrored in a very blue CMR point. Even restricting the ET sample to the “oldest” part of the ET population, i.e. the ET objects for which the value of the $D_n(4000)$ is higher than 1.45 (open circles in figure 12) does not change very significantly the situation, although the CMR for these objects is slightly redder than that of the full ET sample.

The single-color, multi-color, and spectroscopically selected samples of early-type galaxies we have obtained are not independent, having some 60% of galaxies in common, and

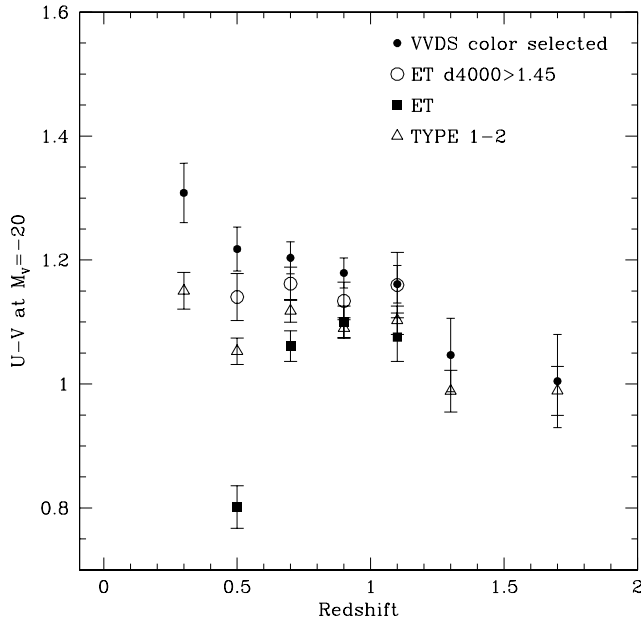


Fig. 12. Color evolution for four classes of objects as measured by the value of the intercept of the CMR at $M_V = -20$. Small filled circles are the VVDS color selected data (as in figure 4); open triangles are the photometric early-type population; filled squares are the ET population; open circles are the “oldest” part of the ET population, i.e. the ET objects for which the value of the $D_n(4000)$ is higher than 1.45.

therefore a certain degree of similarity in the various color-magnitude relations we have derived is to be expected. But we see from figure 12 how the red sample, including some 40% contamination from actively star-forming galaxies, and the subset of the “oldest” ET galaxies, composed exclusively by galaxies with an old stellar population and no current star-formation activity, are described by essentially the same CMR, over a rather large redshift interval. These findings support the conclusion that the average color of the red objects, as measured by the CMR value at fixed luminosity, is not a very sensitive indicator for measuring the evolution of the early-type galaxy population.

This important issue deserves extended analysis. In future papers we will study the spectral classification in more detail and expand our analysis on the effects that different sample selection criteria can have on the inferred properties of the early- and late-type galaxy populations.

8. Summary and conclusions

In this paper we have conducted the study of the rest-frame color distributions on a sample of 6291 galaxies from the first epoch VVDS.

We find that the well-studied local bimodal distribution is still present at previously unexplored redshifts up to $z \sim 2$.

Given the large interval of redshift and luminosity spanned by our sample, we were able to study also the dependence of rest-frame colors distributions on these quantities. We have shown how, at each redshift, faint galaxies are bluer than the

luminous ones. Moreover, at any given luminosity, galaxies become bluer as redshift increases and the amount of this effect is quite independent on the luminosity. This result extends for the first time the findings of previous redshift surveys significantly over the $z \approx 1$ limit. We have extended up to $z \sim 2$ the results of B04 about the evolution of the CMR of red galaxies, finding a slightly fainter evolution and a better agreement with the $z = 0$ point.

We have analyzed the galaxy population which constitute the red-peak of the color distributions finding that a significant fraction is composed of star forming objects. The detailed quantification of this effect at various redshift proves how a simple color selection is not able to reliably isolate early-type objects. The different approach used within the VVDS to isolate galaxy types, based solely on photometric data and local spectral templates fitting, has been shown to have a slightly better capability of isolating passive object than the bimodal one.

Using a robust spectral classification of early-type galaxies in the $D_n(4000)/EW([OII])$ plane, we have demonstrated that a population of galaxies selected only on the basis of their red colors is not only including early-type galaxies with little star formation, but a significant contamination by star-forming galaxies. We conclude that there is no direct equivalence between red-sequence and “dead and old” galaxies, and that selecting galaxies only on the basis of their colors can lead to significant errors in estimating the evolution of old and passively evolving galaxies.

Acknowledgements. This research has been developed within the framework of the VVDS consortium.

This work has been partially supported by the CNRS-INSU and its Programme National de Cosmologie (France), and by Italian Ministry (MIUR) grants COFIN2000 (MM02037133) and COFIN2003 (num.2003020150).

The VLT-VIMOS observations have been carried out on guaranteed time (GTO) allocated by the European Southern Observatory (ESO) to the VIRMOS consortium, under a contractual agreement between the Centre National de la Recherche Scientifique of France, heading a consortium of French and Italian institutes, and ESO, to design, manufacture and test the VIMOS instrument.

References

- Adelberger, K. L., Steidel, C. C., Shapley, A. E., et al. 2004, *ApJ*, 607, 226
- Baldry, I. K., Balogh, M. L., Bower, R., Glazebrook, K., & Nichol, R. C. 2004a, in *AIP Conf. Proc.* 743: The New Cosmology: Conference on Strings and Cosmology, 106–119
- Baldry, I. K., Glazebrook, K., Brinkmann, J., et al. 2004b, *ApJ*, 600, 681
- Balogh, M., Eke, V., Miller, C., et al. 2004, *MNRAS*, 348, 1355
- Balogh, M. L., Morris, S. L., Yee, H. K. C., Carlberg, R. G., & Ellingson, E. 1999, *ApJ*, 527, 54
- Bell, E. F., McIntosh, D. H., Barden, M., et al. 2004a, *ApJ*, 600, L11
- Bell, E. F., Wolf, C., Meisenheimer, K., et al. 2004b, *ApJ*, 608, 752

- Bernardi, M., Sheth, R. K., Annis, J., et al. 2003, *AJ*, 125, 1882
- Bottini, D., Garilli, B., Maccagni, D., et al. 2005, *PASP*, 117, 996
- Bower, R. G., Lucey, J. R., & Ellis, R. S. 1992, *MNRAS*, 254, 601
- Brinchmann, J., Charlot, S., White, S. D. M., et al. 2004, *MNRAS*, 351, 1151
- Bruzual, G. 1983, *ApJ*, 273, 105
- Bruzual, G. & Charlot, S. 2003, *MNRAS*, 344, 1000
- Budavári, T., Connolly, A. J., Szalay, A. S., et al. 2003, *ApJ*, 595, 59
- Bundy, K., Ellis, R. S., Conselice, C. J., et al. 2005, *American Astronomical Society Meeting Abstracts*, 207,
- Cassata, P., Guzzo, L., Franceschini, A., et al. 2006, in preparation
- Cimatti, A., Daddi, E., Mignoli, M., et al. 2002, *A&A*, 381, L68
- Coleman, G. D., Wu, C.-C., & Weedman, D. W. 1980, *ApJS*, 43, 393
- Cowie, L. L., Songaila, A., Hu, E. M., & Cohen, J. G. 1996, *AJ*, 112, 839
- Cucciati, O., Iovino, A., Marinoni, C., et al. 2006, *astro-ph/0603202*
- Dekel, A. & Birnboim, Y. 2006, *MNRAS*, 368, 2
- Dressler, A. 1980, *ApJ*, 236, 351
- Gavazzi, G., Bonfanti, C., Sanvito, G., Boselli, A., & Scoddeggio, M. 2002, *ApJ*, 576, 135
- Gavazzi, G., Boselli, A., Donati, A., Franzetti, P., & Scoddeggio, M. 2003, *A&A*, 400, 451
- Gavazzi, G., Pierini, D., & Boselli, A. 1996, *A&A*, 312, 397
- Giallongo, E., Salimbeni, S., Menci, N., et al. 2005, *ApJ*, 622, 116
- Ilbert, O., Tresse, L., Arnouts, S., et al. 2004, *MNRAS*, 351, 541
- Ilbert, O., Tresse, L., Zucca, E., et al. 2005, *A&A*, 439, 863
- Kauffmann, G., Heckman, T. M., White, S. D. M., et al. 2003a, *MNRAS*, 341, 33
- Kauffmann, G., Heckman, T. M., White, S. D. M., et al. 2003b, *MNRAS*, 341, 54
- Kaviraj, S., Devriendt, E. G., Ferreras, I., Yi, S. K., & Silk, J. 2006, *astro-ph/0602347*
- Kennicutt, R. C. 1998, *ARA&A*, 36, 189
- Kodama, T. & Arimoto, N. 1997, *A&A*, 320, 41
- Kodama, T., Bower, R. G., & Bell, E. F. 1999, *MNRAS*, 306, 561
- Le Fèvre, O., Mellier, Y., McCracken, H. J., et al. 2004, *A&A*, 417, 839
- Le Fèvre, O., Vettolani, G., Garilli, B., et al. 2005, *A&A*, 439, 845
- LeFevre, O., Saisse, M., Mancini, D., et al. 2003, in *Instrument Design and Performance for Optical/Infrared Ground-based Telescopes*. Edited by Iye, Masanori; Moorwood, Alan F. M. *Proceedings of the SPIE*, Volume 4841, pp. 1670-1681 (2003), ed. M. Iye & A. F. M. Moorwood, 1670–1681
- Lilly, S. J., Tresse, L., Hammer, F., Crampton, D., & Le Fèvre, O. 1995, *ApJ*, 455, 108
- McCracken, H. J., Radovich, M., Bertin, E., et al. 2003, *A&A*, 410, 17
- Menci, N., Fontana, A., Giallongo, E., & Salimbeni, S. 2005, *ApJ*, 632, 49
- Meneux, B., Le Fèvre, O., Pollo, A., et al. 2005, *astro-ph/0511656*
- Mignoli, M., Cimatti, A., Zamorani, G., et al. 2005, *A&A*, 437, 883
- Radovich, M., Arnaboldi, M., Ripepi, V., et al. 2004, *A&A*, 417, 51
- Renzini, A. 2006, *astro-ph/0603479*
- Roberts, M. S. & Haynes, M. P. 1994, *ARA&A*, 32, 115
- Salpeter, E. E. 1955, *ApJ*, 121, 161
- Sandage, A. 1986, *A&A*, 161, 89
- Schlegel, D. J., Finkbeiner, D. P., & Davis, M. 1998, *ApJ*, 500, 525
- Scoddeggio, M., Franzetti, P., Garilli, B., et al. 2005, *PASP*, 117, 1284
- Stanford, S. A., Eisenhardt, P. R., & Dickinson, M. 1998, *ApJ*, 492, 461
- Strateva, I., Ivezić, Ž., Knapp, G. R., et al. 2001, *AJ*, 122, 1861
- Tremonti, C. A., Heckman, T. M., Kauffmann, G., et al. 2004, *ApJ*, 613, 898
- Tully, R. B., Mould, J. R., & Aaronson, M. 1982, *ApJ*, 257, 527
- van Dokkum, P. G. & Franx, M. 2001, *ApJ*, 553, 90
- Visvanathan, N. & Sandage, A. 1977, *ApJ*, 216, 214
- Weiner, B. J., Phillips, A. C., Faber, S. M., et al. 2005, *ApJ*, 620, 595
- Zanichelli, A., Garilli, B., Scoddeggio, M., et al. 2005, *PASP*, 117, 1271
- Zucca, E., Ilbert, O., Bardelli, S., et al. 2005, *astro-ph/0506393*